Provisional chapter

Kinetic Model of Development and Aging of Artificial Skin Based on Analysis of Microscopy Data

Paola Pesantez-Cabrera, Cläre von Neubeck, Marianne B. Sowa and John H. Miller

Additional information is available at the end of the chapter

Abstract

Artificial human skin is available commercially or can be grown in the laboratory from established cell lines. Standard microscopy techniques show that artificial human skin has a fully developed basement membrane that separates an epidermis with the corneal, granular, spinosal, and basal layers from a dermis consisting of fibroblasts in an extracellular matrix. In this chapter, we show how modeling can integrate microscopy data to obtain a better understanding of the development and aging of artificial human skin. We use the time-dependent structural information predicted by our model to show how irradiation with an electron beam at different times in the life of artificial human skin affects the amount of energy deposited in different layers of the tissue. Experimental studies of this type will enable a better understanding of how different cell types in human skin contribute to overall tissue response to ionizing radiation.

Keywords: artificial human skin, kinetic model, radiation exposure, protection by corneal layer, selective irradiation of epidermis

1. Introduction

Engineered human tissues provide a bridge between in vivo and in vitro studies by enabling the investigation of fundamental cellular mechanisms at a level of detail that is not possible with whole-animal models, while providing a tissue-like context specific to the organ under investigation (reviewed in reference [1]). Such models are routinely used for toxicology and radiation studies [2–6].

Artificial human skin, a well-known example of engineered human tissue, is available commercially but can also be developed from human cell lines in the laboratory [7, 8]. EpiDermFT™ (MatTek, Ashland, VA) is a widely used commercial product that exhibits a fully developed basement membrane that separates the epidermis, with keratinocytes in the corneal, granular, spinosal, and basal layers, from the dermis consisting of fibroblasts in an extracellular matrix.

Microbeam irradiation of EpiDermFT™ and similar skin-tissue models showed that skin exhibits a "radiation-induced bystander effect" (reviewed in reference [9]); cells that are not directly damaged by ionizing particles in the beam nevertheless exhibit biological responses similar to cell that receive direct damage. Hence, it appears that Interactionslayers and cell types plays a role among different layers and cell types play a role in the response of skin to ionizing radiation. Experiments that vary the dose delivered to different layers of artificial skin will contribute to our understand of these interactions.

Cole and coworker [10] showed that, due to its limited penetration in biological materials, the sensitivity of different components of a biological system can be investigated by low-voltage electron-beam irradiation. Recognizing that this technique could be useful in a layered system such as the skin, we calculated the penetration of electron beams of various energies into artificial skin [11] as a basis for the design of experimental studies.

We immediately realized that a detailed analysis of microscopic images of artificial skin was required to ensure accurate calculation of penetration depths. In this chapter, we trace the evolution of our analysis of microscopy data for the purpose of modeling the interaction of artificial skin with electron-beam irradiation. Initially, our focus was on irradiation at a fixed time dictated by experimental procedures coupled with the purchase of EpiDermFT™ from MatTek. Later, we realized that earlier delivery by MatTek and in-house production of artificial skin enabled irradiation studies at different stages in the development of the tissue model. This realization encouraged us to develop a kinetic model of artificial-skin growth and aging that would support simulations of electron-beam exposure at any time during its life cycle.

2. Morphology of the fully developed epidermis of artificial skin

Radiation biology experiments on EpiDermFT™ [6, 12, 14] are usually preformed approximately 3 weeks postseeding of the keratinocytes onto the dermal substrate. At this time, images such as those shown in **Figure 1** reveal the morphology of the mature skin model.

Image A in **Figure 1** (kindly provided by MatTek [13]) uses hematoxylin and eosin (H&E) staining to show the structure of EpiDermFT™ at the time of shipping, about 17 days postseeding of keratinocytes onto the dermal substrate. Horizontal lines added by us approximately delineate layers of the epidermis and suggest that, on average, the spinosal layer is about twice as thick as the basal layer, and granular layers have about the same thickness as the basal layer. Using the scale mark shown in **Figure 1A**, we estimate that the basal, spinosal, and granular layers are about 17, 37, and 17 μm thick, respectively. In this chapter, we refer to

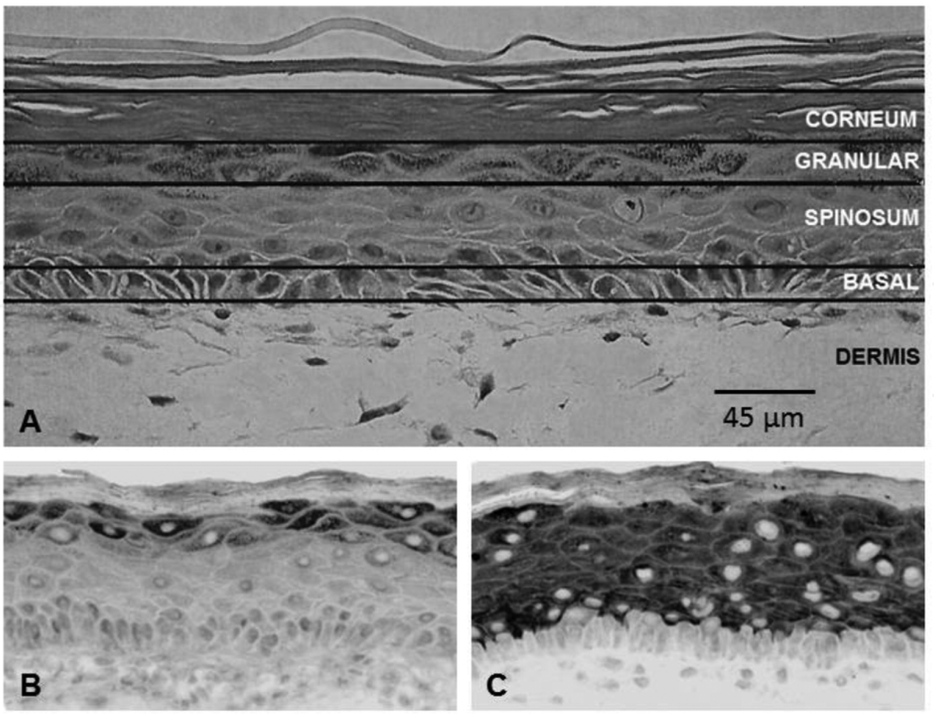

Figure 1. Representative histological sections showing morphology and differentiation in the EpiDermFT™ skin model 17–20 days after the seeding of keratinocytes onto the dermal substrate. Samples A, B, and C were stained for eosin, filaggrin, and keratin10, respectively. For filaggrin and keratin10, positive DAB staining appears dark in the image. All tissues were counterstained with hematoxylin. The scale bar in A applies to B and C as well.

the combined basal, spinosal, and granular layers as the "viable" epidermis to contrast it from the corneal layer of dead cells.

Cells in the stratum corneum have lost most of their intercellular adhesion so that even careful sample handling is likely to induce small air gaps such as those seen in the lower part of the corneal layer in **Figure 1A**. Experimental procedures involved in microscope slide preparation can destabilize the stratum corneum and are, most likely, responsible for large air gaps, such as those seen in the upper part of the corneal layer in **Figure 1A**. Consequently, these images are not a reliable source of data on corneal thickness.

MatTek also provided valuable information about the production of their human skin model. A nutrient layer is seeded with neonatal foreskin basal cells. It is unlikely that this population contains stem cells; hence, the basal layer has finite replication capacity due to transiently amplifying (TA) cell, about 80% of which are in a resting state at any one time. Ca+ ions in the nutrient layer diffuse into the epidermis but are trapped beneath the corneal layer, which creates a Ca+ gradient since water can diffuse into the liquid-air interface. As in normal skin, this Ca+ gradient is most likely responsible for the differentiation of keratinocytes as they are pushed toward the stratum corneum by cell replication in the basal layer.

Images B and C in **Figure 1** are prepared in Dr. Sowa's laboratory approximately 3 weeks postseeding of keratinocytes onto the dermal substrate [14]. When EpiDermFT™ skin samples were received from MatTek, they were placed in 2 ml of maintenance media and incubated at

37°C and 5% CO^2 as the manufacturer instructed. After 2 days, tissues were fixed in 4% paraformaldehyde, dehydrated, and embedded in paraffin wax using standard methods [15].

Five-micrometer sections were prepared using a Leica microtome and mounted onto coated slides (IMEB, Inc., San Marcos, CA). Sections were deparaffinized in xylene and rehydrated via a series of alcohol rinses. Sections were processed for antigen retrieval by immersion in a citrate acid solution (pH 6.0, 99°C) for 30 min, followed by immersion in 3% H_2O_2 for 10 min to block endogenous peroxidase activity. Slides were then washed three times in phosphate-buffered saline (PBS) for 10 min, blocked with 0.3% bovine serum albumin (BSA) for 1 h, and incubated in the primary antibody overnight at 4°C.

Immunofluorescence staining was performed in triplicate to ensure consistent results. Individual tissue sections were imaged using a Nikon Eclipse TE300 microscope with a Nikon Plan APO VC 60x/1.20 water immersion objective. A Retiga 1300 cooled charge-coupled device (CCD) camera (Qimaging) controlled by QCapture software was used to acquire the image. Image processing was performed in Image J (NIH; Bethesda, MD).

Images B and C in **Figure 1** show differentiation profiles for nonirradiated EpiDermFT™ skin-model samples using filaggrin and Keratin10, respectively. Filaggrin-positive staining defines the granular layer only. Keratin10-positive staining defines the combined spinosum and granular layers but is excluded from the basal layer. Image B seems to indicate that the granular layer contains cells both with and without a nucleus. Furthermore, granular cells with nuclei appear to be adjacent to the stratum corneum. Image C shows that cells in the spinosal layer vary in size with smaller cells nearer to the basal layer. We interpret this as evidence for cell growth as keratinocytes traverse the spinosal layer.

Thicknesses of the basal, spinosal, and granular layers revealed by images B and C in **Figure 1** are roughly in the same proportions as that suggested by the horizontal lines in **Figure 1A**. However, absolute thicknesses cannot be compared due to both sample variability and differences in ages of the sample when the images were acquired. Due to the time spent in shipping and equilibration, images B and C are for samples approximately 4 days older than the sample shown in **Figure 1A**. A significant shrinkage of the viable epidermis (basal, spinosal, and granular layers) during this time was reported in reference [14].

The thickness of the viable epidermis at any given point is stochastic, depending on the particular arrangement of cells in the basal, spinosal, and granular layers. One way to average over this intrinsic variability is to measure area over a fixed width, also called "field of view." This technique was used in reference [14] to measure the thickness of the viable epidermis in samples stained using a standard H&E protocol [15]. As stated above, MatTek normally ships EpiDermFT™ 17 days postseeding of keratinocytes onto the dermal substrate; however, they will ship samples at earlier time points in sample production if requested. Early shipment was desirable for some of the radiation biology studies conducted by Sowa and coworkers [9, 14], which allowed them to measure the thickness viable layers of the epidermis starting on day 17 postseeding. Results of these measurements are shown in **Table 1**.

Day	Relative thickness
17	1.00 ± 0.04
18	1.14 ± 0.06
19	0.93 ± 0.05
20	0.93 ± 0.06
21	0.76 ± 0.04
22	0.90 ± 0.16
23	0.64 ± 0.08
24	0.42 ± 0.06

Table 1. Relative thickness of the viable epidermis as a function of sample age.

In **Table 1**, the data have been normalized by the mean of areas observed on day 17 and uncertainties are ±1 standard deviation. Shrinkage starts between days 18 and 19 after an increase in thickness between days 17 and 18. With the exception of day 21, shrinkage of the viable epidermis is relatively minor between days 19 and 22. After day 22, shrinkage is linear with the thickness decreasing about 25% each day.

The biological reason for these changes in the thickness of the combined basal, spinosal, and granular layers is not clear. This is particularly true between days 17 and 22 when the variation is not systemic. The severe shrinkage after day 22 suggests that a dramatic change has occurred in the viable epidermis, possibly due to the exhaustion of replication capacity in the basal layer. If we assume that shrinkage is uniform across the basal, spinosal, and granular layers, we can easily include this shrinkage when we convert cell count from our kinetic model into layer thickness.

3. Properties of artificial skin epidermis revealed by confocal microscopy

The microscope images described in the previous section provide the quantitative information needed to model the viable layers of EpiDermFT™ skin-tissue samples at about 20 days after keratinocytes were seeded onto the dermal substrate. These images of stained vertical slices through the epidermis frequently display large air gaps in the corneal layer, such as those shown in **Figure 1A**, which we attribute to sample preparation. Hence, these images cannot provide reliable quantitative information about the thickness of the corneal layer. To obtain this type of information, we analyzed three-dimensional (3D) confocal microscopy of live samples [6].

Samples were stained overnight with SYTO13 and SYTO59 fluorescent nucleic acid stains (Invitrogen). Two colors (red and green) were chosen because of their high contrast and strong overlap with the excitation lasers of the confocal microscope. Both dyes were used at a final concentration of 10 μM in 3 ml of media. Stained samples were washed with PBS and placed in a 35-mm culture plate containing sufficient PBS to cover the tissue. To minimize sample movement during imaging, samples were placed on a thin coating of autoclaved petroleum

jelly prior to the addition of the PBS. Images were acquired in 1-μm z-steps on a Zeiss laser scanning microscope (LSM) 710 scanning head confocal microscope with a Zeiss plan apo 40×/1.1 objective. Excitation lasers were 488 and 633 nm for the green and red emission channels, respectively. Laser dwell times were 1.27 μs for both channels. Two-dimensional (2D) and 3D image analyses were carried out using Volocity (Perkin Elmer, Waltham, MA).

Confocal microscopy of EpiDermFT™ skin-model samples treated with fluorescent nucleic acid stains, as described above, revealed the location of nuclei in the samples. **Figure 2** illustrates a detailed analysis of a confocal microscopy image designed to measure the thicknesses of the corneal layer and the viable epidermis at 20 days after seeding of keratinocytes onto the dermal substrate.

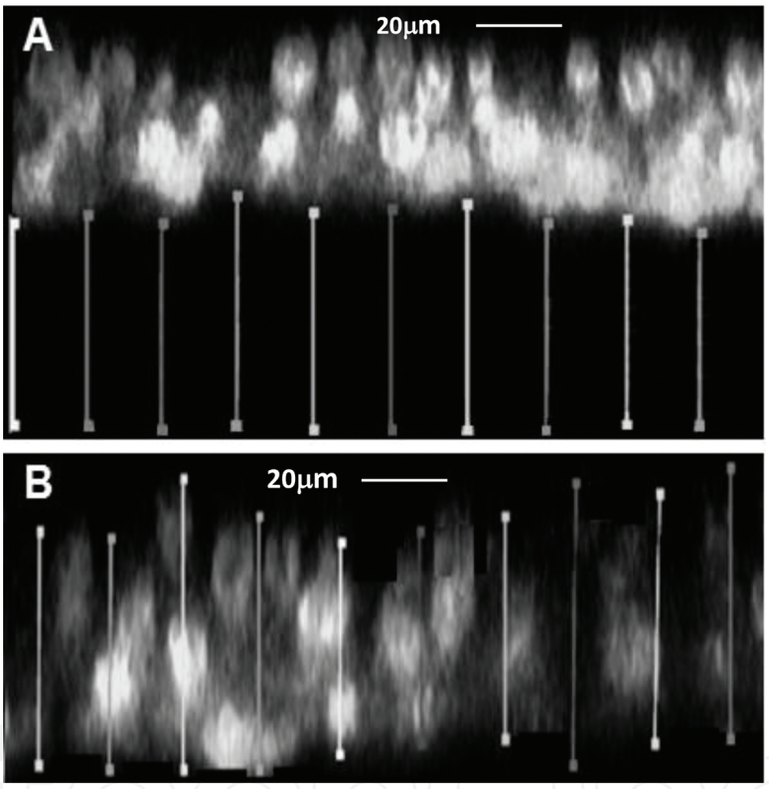

Figure 2. Side view of a 3D image of EpiDermFT™ epidermis obtained by confocal microscopy following treatment with fluorescent nucleic acid stains at 20 days after seeding of keratinocytes onto the dermal substrate. Vertical lines illustrate repeated measurements of the thickness of regions that did (B) and did not (A) take up the stain.

Vertical lines in panel B of **Figure 2**, which span the thickness of the epidermis where stained nuclei were observed by confocal microscopy, have an average length of 45.2 ± 0.7 μm. This distance agrees with the thickness of the combined basal and spinosal layers from **Figure 1A** after we allow for shrinkage between days 17 and 20, shown in **Table 1** (0.93 ± 0.06 × 54 μm = 50.2 ± 3.2 μm). For this association between information derived by two different types of microscopy to be valid, we must assume that granular cells do not take up the DNA stains, even though, as mentioned above, H&E-stained tissue sections seem to show nuclei in some granular cells.

Vertical lines in panel A of **Figure 2**, which span the thickness of the epidermis where DNA staining is not observed, have an average length of 55.0 ± 0.41 μm. Based on the assumption that granular cells do not take up the DNA stain, the combined granular and corneal layers have a thickness of 55.0 ± 0.41 μm on day 20. Assuming further that the shrinkage observed on day 20 is uniform across the viable epidermis, we calculate the thickness of 16 ± 1 μm (17 × 0.93 ± 0.06) for the granular layer on day 20, which allows us to estimate the corneal-layer thickness as 39 ± 1.41 μm (55 ± 0.41 – 16 ± 1) on day 20.

By itself, this estimate of the corneal-layer thickness on day 20 is not extremely useful; however, in conjunction with a kinetic model for the number of cells in the stratum corneum, it can be used to estimate the thickness of the corneal layer at all times after its first appearance 7–10 days postseeding of keratinocytes onto the dermal substrate. If we assume that the thickness of corneal cells is constant, then the ratio of cell number to layer thickness on day 20 is the same at all times. Our kinetic model, described in Section 5, was developed to predict corneal cell populations, which can be converted into corneal thickness.

Figure 3 shows the distribution of nuclei in the region of the epidermis that took up the DNA stains. To determine the number of nuclei in a specific volume at a specific depth, Z-stacks of optical sections were reconstructed in 10-μm sections starting at the bottom of the basal layer. Individual nuclei were identified by a threshold on the florescence intensity and the number in each 10-μm section was counted. The 2D image area was approximately 60,000 μm^2.

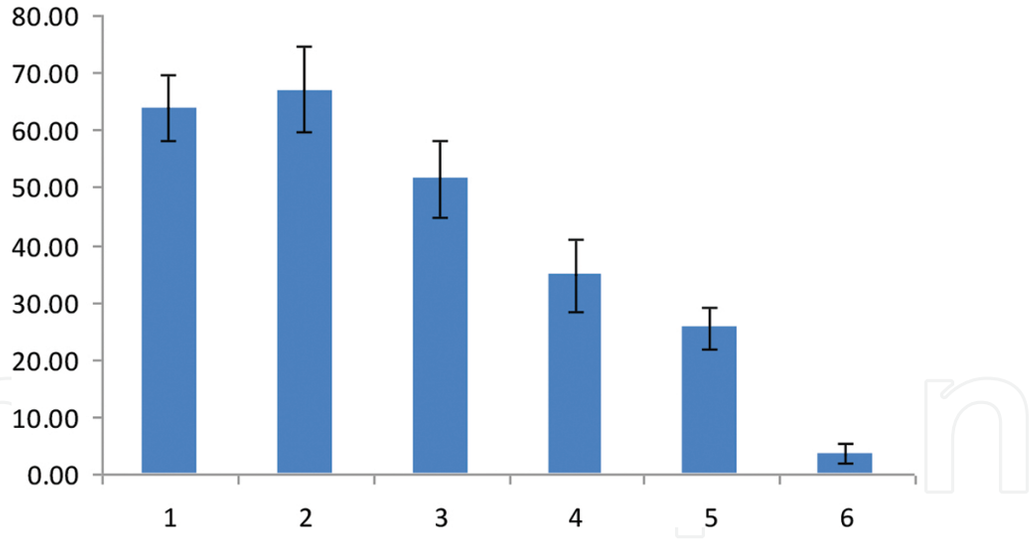

Figure 3. Number of nuclei (vertical axis) in successive 10-mm thick slices numbered 1-6 on the horizontal axis of a 3D confocal microscope image of EpiDermFT™ skin model starting on the basement membrane and ending in the granular layer.

The first two bars of the histogram in **Figure 3** are counts of nuclei in the basal layer and the start of the spinosal layer. Between 20 and 50 μm above the basal membrane, the number of nuclei counted in 10-μm sections decreases linearly. We interpret this decrease in nuclei per unit area as evidence for increasing cell volume as keratinocytes pass through the spinosal layer. A significant departure from this linear behavior occurs in the count of nuclei between

50 and 60 μm above the basal membrane. We associate the small number of nuclei in this 10-μm section as a small number of cells at the base of the granular layer that took up the DNA stain. The deviation from the linearity of nuclei counts between 50 and 60 μm is interpreted as a decrease in the number of cell susceptible to DNA staining, not to an increase in cell volume. Our kinetic model assumes that keratinocytes in the granular layer have the same volume as those cells at the top of the spinosal layer.

4. Simulation of electron-beam penetration into skin

PITS [16] is a radiation transport code that performs an event-by-event simulation of charged particles transferring their kinetic energy to electronic excitations of a medium. Simulated tracks are data objects containing, among other things, the Cartesian coordinates of energy deposition events. Properties of elastic collisions are not retained in the track object except as they influence the position of inelastic interactions in the stopping medium. Condensed phase effects [17] are included as described by Wilson et al. [18]. Primary electrons and all generations of secondary electrons are followed until their energy falls below 10 eV, the lowest ionization threshold in Dingfelder's model [17], after which residual kinetic energy is assigned to a final transfer point cast in an isotopically random direction and at an exponentially random distance.

For each electron-beam energy considered, 10^5 independent primary electrons were simulated as they transferred their energy to a liquid-water medium. For layers of the epidermis containing live cells, liquid-water provides a reasonable approximation due to their high water content; however, this approximation may not be valid for the corneal layer due to the low water content and small air gaps.

The density of the cellular material in the stratum corneum is slightly greater than water [19] but the presence of air gaps makes the average corneal density less than that of its cellular material. To allow for these competing factors in determining a water thickness with equivalent mass per unit area as the corneal layer, we used microscope images such as in **Figure 4**, to quantify the relative area of small air gaps. We consider these small air gaps as intrinsic to the corneal layer under normal sample handling during experiments.

Microscope slides of Vertical slices through EpiDermFT™ were prepared by methods described in Section 2 and stained with H&E (IMEB, Inc.). A Nikon Eclipse TE300 inverted microscope with a Nikon Plan APO 20/0.75 objective was used to image individual tissue slices. A Retiga 1300 cooled CCD camera (Qimaging) controlled by Volocity Acquisition (Improvision) software was used to acquire images and to take area measurements. A 12-bit gray scale of intensity determined the relative proportions of high- and low-density materials in the image. High-density material was associated with pixels with normalized gray scale intensity between 0.5 and 15%. The air pockets in the stratum corneum layer were associated with pixels in the 23–100% gray level intensity range.

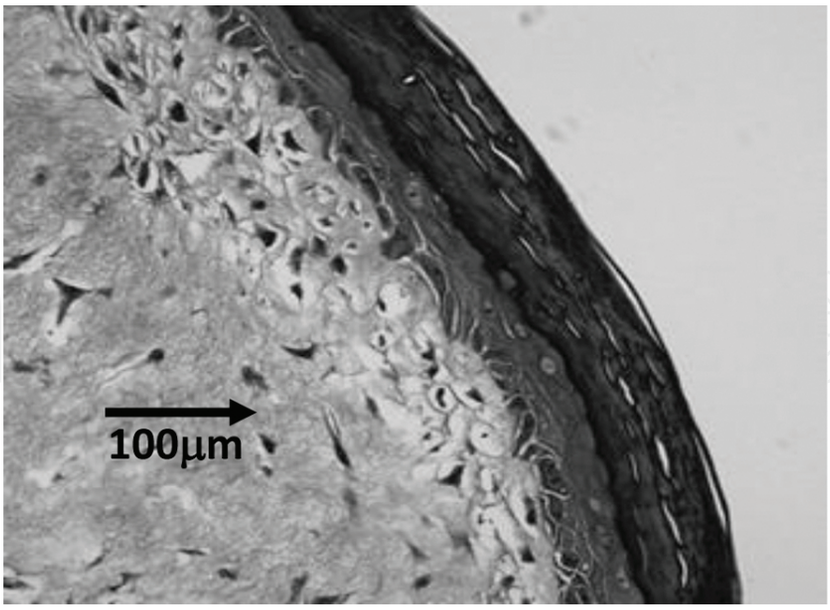

Figure 4. Microscope image of a vertical slice through the EpiDermFT™ skin-tissue model showing small air gaps in the corneal layer.

Area measurements of high and low intensity performed on 14 distinct regions of the stratum corneum gave a mean relative area of low-density material of 9.53% with a standard deviation of the mean 0.81%. Given the large number of cross-sections sampled, it is reasonable to assume that the relative volume of air in the stratum corneum is about 10%.

Weigand et al. [19] measured the buoyant density of the stratum corneum cellular material from Caucasian and Black subjects by several techniques. They concluded that the sucrose density gradient method gave values closest to that of the natural state. Averages of repeated experiments with Caucasian samples, which should apply to the EpiDermFT™ skin model, ranged from 1.075 to 1.145 g/ml. Consequently, the increase in equivalent water thickness to account for the higher density of cellular material in the stratum corneum is approximately equal to the decrease in the thickness of water to account for air pockets. We conclude from these results that calculations of electron-beam penetration in a uniform water medium provide a reasonable approximation to the penetration of the EpiDermFT™ skin model, including the corneal layer.

Figure 5 shows the cumulative probability distribution of samples of the largest *z*-coordinate of energy transfer points in simulated tracks of 90-keV electrons stopping in a uniform liquid-water medium. Percentile points of this distribution give the thickness of water required to stop a specified fraction of electrons injected into the medium. For example, about 40 μm of water is required to stop about half of the electrons in a 90-keV beam. The dashed curve in **Figure 5** shows the fraction of beam energy deposited by events not exceeding a specified depth. The point a zero depth shows that about 12% of the beam energy is backscattered. By interpolation between calculations at 60 and 70 μm, we estimate that 4% of the beam energy is deposited at depths that exceed the 90th percentile of penetration.

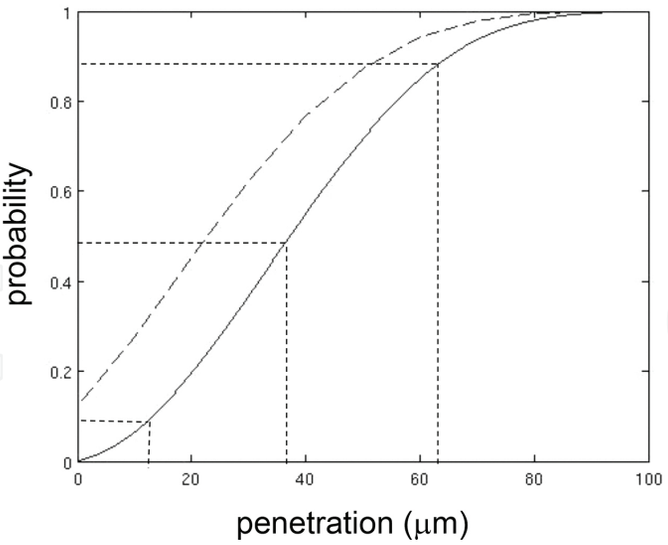

Figure 5. Penetration and energy deposited by a 90-keV electron beam in water. Solid curve is the cumulative probability of maximum *z*-coordinate of energy transfer points. Intersecting horizontal and vertical dashed lines show 10th, 50th, and 90th percentiles of penetration. Dashed curve shows the fraction of beam energy deposited by events not exceeding a specified depth, with the point a zero depth showing the fraction of beam energy backscattered. Reprinted with permission from Radiation Research.

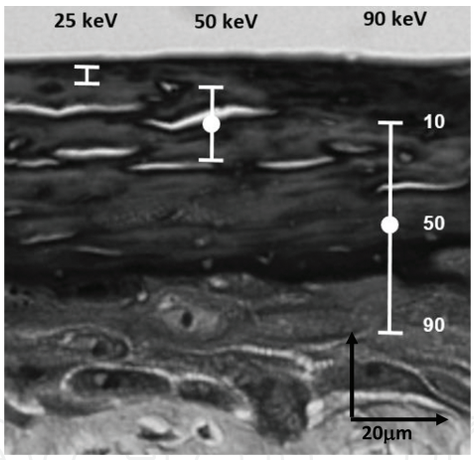

Figure 6. Microscope image of a vertical slice through the EpiDermFT™ skin-tissue model overlay showing calculated penetration of 25-, 50-, and 90-keV electron beams. Bars cover the 10–90th percentile of penetration with the 50th percentile at the center. Reprinted with permission from Radiation Research.

The overlay in **Figure 6** shows the penetration of 25-, 50-, and 90-keV electron beams superimposed on a microscope image of a vertical slice through the EpiDermFT™ skin model. The uncertainty bar is centered on Z_{p50} and the upper and lower extremes are Z_{p10} and Z_{p90}, respectively, where Z_{pX} is the depth to which X% of the electron beam is expected to penetrate. It is clear from the overlay in **Figure 6** that beam energies near 90 keV are required to irradiate keratinocytes in the epidermis that are undergoing active cell division, which is usually the population of greatest interest in radiation biology.

5. Kinetic model of epidermis formation and aging

In this section, we present a kinetic model for the development of the basal, spinosal, granular, and corneal layers of the EpiDermFT™ skin-tissue model. The main purpose for developing this model is to estimate the corneal layer thickness from the start of its formation 7–10 days after seeding of keratinocytes onto the dermal substrate to the end of the useful life of the sample for radiation biology studies due to shrinkage. Our model predicts the kinetics of the number cells in the corneal layer. If we assume that the thickness of a corneal cell is constant, then the measure of corneal layer thickness at 20 days (see Section 3) can be used to convert cell count into layer thickness at any time.

A kinetic model of artificial-skin development was reported in reference [9] that focused on the viable epidermis for comparison with experimental studies of skin homeostasis after exposure to ionizing radiation [9, 14]. The model in reference [9] starts with a rapid expansion of TA basal cells, with the population increasing sixfold in about 12 days. By contrast, the kinetic model described here starts with a confluent monolayer of the basal cells and the total basal-cell population, consisting of cycling TAs, noncycling TAs with replication potential, and the basal cells that have exhausted their replication capacity, is constant throughout the simulation.

As in reference [9], we assume that TA cells exhaust their replication capacity after five to three cycles, but the current model includes the information from MatTek that only about 20% of TA cells are cycling at any given time. This means that as individual TA cells exhaust their replication capacity, they are replaced by a TA cell with full replication capacity that has been held in reserve. The biological mechanism for delayed cycling of TA cells with replication capacity is unclear; however, as **Figure 7** shows, this modeling assumption allows the cycling TA population to be constant throughout most of our kinetic simulation. Replication in the

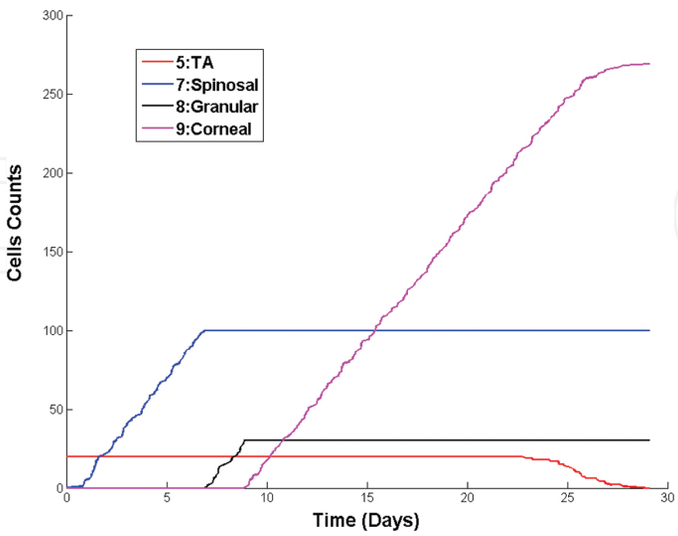

Figure 7. Predicted kinetics of cell count in the basal (orange), spinosal (blue), granular (black), and corneal (red) layers of the epidermis of an artificial-skin tissue, starting from the time with the basal layer is confluent.

basal layer goes to zero after about day 23 when reserve replication capacity is no longer available.

In the current model, the differentiation of keratinocytes is determined by their height above the basement membrane. We think this more correctly models differentiation driven by a Ca + gradient than the purely time-dependent transitions of the kinetic model in reference [9]. Height-dependent differentiation means that a spinosal cell is the consequence of each TA-cell replication. TA cycling produces two daughter TA cells, but some basal cells must move to the spinosal layer because the basal-cell layer is confluent

As can be seen in **Figure 7**, the spinosal-cell population is non-zero after the first TA-cell replication, which occurs at TA cycle time chosen randomly from a lognormal distribution with a mean TA cycle time of 31.2 h. The lognormal distribution of TA cycle times and its variance are the same as in reference [9] but the mean TA cycle time in the current model is significantly shorter. A shorter mean cycling time for TA cells in the current model is a direct consequence of our assumption, based on information from MatTek [15] that only about 20% of TA cell with replication potential are cycling at any given time. Consequently, a shorter mean cycling time is required to generate complete spinosal and granular layers 7–10 days postseeding of keratinocytes than is the case when all TAs with replication potential are cycling.

In our kinetic model, the corneal layer begins to form as soon as the granular layer reaches its full thickness. Exposure to air is crucial to the formation of a corneal layer but this requirement is not explicitly included in our model. **Figure 7** also shows that the rates of increase of spinosal, granular and corneal cell populations are all nearly equal, aside from random fluctuations, to a constant value determined by the rate of TA-cell replication in the basal layer. The rates of increase in the thickness of the spinosal, granular, and corneal layers are not the same because the volumes of individual cells in those layers are different. In addition, the volume of a spinosal cells is increasing with time since it entered the stratum spinosum.

Sharp transitions between increasing and constant cell populations in the spinosal and granular layers are an artifact of our model in which cell type is determined by a specified height of the cell above the basement membrane. If a TA cycle, which adds a cell to the stratum spinosum, makes the upper boundary of the spinosal layer exceed the height above the basement membrane allowed for spinosal cells, the oldest cell in the current stratum spinosum becomes a granular cell. A similar modeling assumption governs the transition of granular to corneal cells.

The transition between linearly increasing to constant corneal cell population is not sharp. This transition mirrors the loss of replication capacity in the basal layer, which occurs over about a 4-day time period. In **Figure 7**, this loss of replication capacity occurs between days 23 and 29. Various model parameters, including the mean TA cycle time and the fraction of cycling TA cells, determine the duration of replication capacity in the basal layer. parameters affect the time when replication capacity is exhausted relative seeding of keratinocytes onto the dermal substrate. We think that the decay of replication seen in **Figure 7** is reasonable because it correlates roughly with the onset of significant shrinkage of the viable epidermis observed

experimentally [14] (see **Table 1**). After replication capacity is exhausted, cell count in all layers is constant. Cell count in the basal layer is always constant but transitions between cycling, resting with replication potential, and sterile TA cells occur throughout the kinetic simulation.

Even though cell count in the viable epidermis remains constant after complete formation of spinosal and granular layers, its thickness is not constant due to shrinkage. On converting cell count to layer thickness after shrinkage begins, we assume that its effect is uniform across all three layers, basal, spinosal, and granular, of the viable epidermis. After day 18, we assume that the volume of all cells in the viable epidermis decreases in accordance with the shrinkage fractions in **Table 1**. Although no data are available, it seems reasonable that corneal cells do not shrink since they are dead and have lost most of their water content. Hence, we can use the corneal thickness of 39 ± 1.41 μm deduced from confocal microscopy on day 20 to convert corneal cell count to corneal thickness at any time after its appearance, about day 8.5 shown in **Figure 7**.

A typical simulation begins by assigning a maximum of 3, 4, or 5 replications randomly to 100 basal cells, 20 of which are chosen randomly to be expressing this replication potential at the beginning of the simulation. The 20 active TA cells are assigned cycle times randomly drawn from a lognormal distribution with a variance of 0.2 and a mean cycling time chosen to generate complete spinosal and granular layers 7–10 days postseeding of keratinocytes, as reported by MatTek [15].

The active TA cell with the shortest cycling time is selected for replication, which forces a randomly selected TA cell off the basement membrane to become a spinosal cell and leaves a TA cell on the basement membrane that is capable of one less replication. The current simulation time is upgraded and a new random cycle time is assigned to the TA cell that just replicated, if it still has replication capability. If not, the TA cell that just replicated becomes a permanently resting TA cell and is replaced by a TA cell that can replicate, if the pool of TA cells with replication capacity is not empty.

If we knew the growth rate of spinosal cells, we would assign the spinosal cell generated by TA-cell replication a birth time equal to the current simulation time and volume equal to that of a basal cell. The age of any preexisting spinosal cells would increase by the TA cycle time and their volume would increase to reflect growth during that cycle time. The growth rate of spinosal cells cannot be determined from the available data; however, as discussed below, the difference in the volume of spinosal cells at different heights in the spinosal layer can be estimated from the data in **Figure 3**. This allows us to calculate the average volume of a spinosal cell, which we assign to all cells in the spinosal population.

After each TA-cell replication, we find the active TA cells with the shortest cycling time, which determine the size of the next time step in the simulation. However, before that time step can be taken, we must determine if a spinosal cell needs to transition to a granular cell, based on the current thickness of the spinosal layer. From the microscopy images in **Figure 1**, it is clear that the spinosal and granular layers are confluent; hence, the volume of the spinosal and granular layers at any time in the simulation is the sum of the volumes of the cells in those layers. The current thickness of the spinosal and granular layers is their current total volume

divided by the area of skin being simulated, which is 100 times the cross-sectional area of a basal cell. If the current thickness of the spinosal layer exceeds the observed thickness of a fully formed spinosal layer, a spinosal cell transitions to a granular cell with an appropriate average volume change.

We assume that all granular cells have the same volume that does not change with time. As with the spinosal layer, we estimate the current thickness of the granular layer as its population volume divided by the simulation area. If this total thickness exceeds that observed for a fully developed granular layer, a granular cell transitions to a corneal cell. Updating the count of corneal cells, if needed, completes a simulation time step.

To conduct the series of steps in the simulation described above requires parameters derived from the analysis of microcopy data. A vertical slice through the skin-tissue model imaged by H&E staining 17 days postseeding of keratinocytes allowed us to estimate values of 17, 37, and 17 μm for the thickness of the basal, spinosal, and granular layers, respectively, after they are fully developed and before shrinkage begins. We compare these thicknesses to layer thicknesses after each time step of the simulation to determine if changes in cellular populations are needed. To conduct this test, we need the area of artificial skin being modeled. In our simulation, the basal-cell layer is always a confluent monolayer; hence, the mean separation of basal-cell nuclei, observed to be 14.9 μm by confocal microscopy after DNA staining [6], is an estimate of the mean lateral thickness of the basal cells. By this method, we estimate the cross-sectional area of the basal cells to be 14.9 μm^2, so a typical area of skin in our simulations is $100 \times (14.9\ \mu m)^2 = 2.22 \times 10^4\ \mu m^2$.

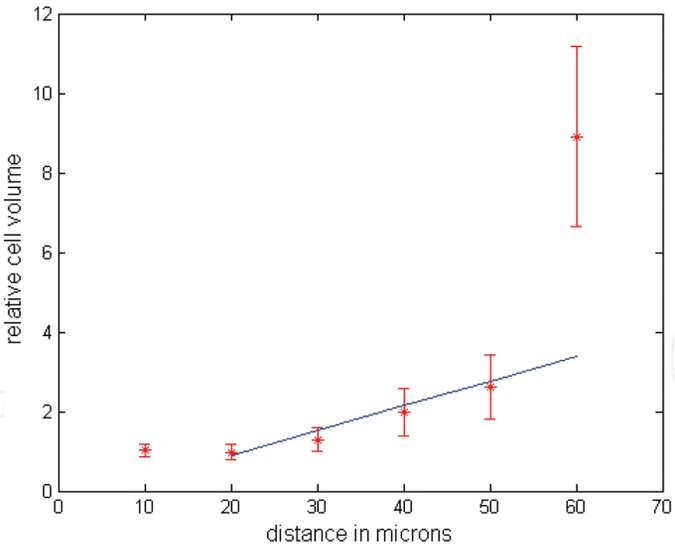

Figure 8. Change in the volume per cell as a function of distance above the basement membrane. Data were normalized to the volume of the basal cells by averaging the results for slices of 3D confocal microscopy data 0–10 and 10–20 μm above the basement membrane. The line fit to data at heights greater than 20 μm mainly reflects the changing volume of spinosal cells.

The analysis of microcopy data discussed in this chapter does not yield a direct measure of spinosal-cell growth rate. However, the analysis of confocal microcopy data for the distribution

of nuclei as a function of height above the basement membrane, shown in **Figure 3**, can be used to estimate the change in spinosal-cell volume as a function of height above the basement membrane. As discussed in Section 3, the number of nuclei at various heights above the basement membrane was estimated by counting the number of stained object in a 10-μm slice with an image area of 60,000 μm^2. Dividing the volume of the slice, 600,000 μm^3, by the observed count, we get an estimate of the volume per cell, assuming that each cell has a single nucleus. The counts of nuclei in slices 10 and 20 μm above the basement membrane mainly reflect the volume of the basal cells. The average of calculated volume per cell at 10 and 20 μm was used to normalize the data; hence, the data shown in **Figure 8** are the relative change in cell volume versus height above the basement membrane.

The linear trend in the relative volume per cell between 20 and 50 μm above the basement membrane is not reflected in the data at 60 μm. Based on **Figure 1A** and allowing for shrinkage on day 20 (see **Table 1**), we estimate that the combined thickness of the basal and spinosal layers on day 20, when the confocal data were obtained, is 50.2 μm. Hence, the data shown in **Figure 8** at 60 μm are mainly due to nuclear staining in the granular layer and reflect the uptake of the DNA stains more than the size of cells in the granular layer.

As the results in **Figure 8** show, a linear model is reasonable for the change of spinosal-cell volume as a function of their height in that layer. We express this model as

$$v_s(h) = v_b(1 + (g-1)(h - \Delta_b)/\Delta_s \tag{1}$$

where v_b is the volume of a basal cell, $v_s(h)$ is the volume of a spinosal cell at height h above the basement membrane, Δ_b is the thickness of the basal layer, and Δ_s is the total thickness of the spinosal layer. The parameter g is the ratio of the volume of a granular cell to a basal cell, which can be verified by applying Eq. (1) at the maximum height of the spinosal layer. This parameter can be estimated by setting $(g\text{-}1)/\Delta_s$ to the slope of the linear fit shown in **Figure 8**, which gives a value of $g = 3.32$.

Equation (1) is not directly useful in our kinetic simulation because we do not know the height above the basement membrane of individual cells in the spinosal layer; however, since $v_s(h)$ is linear, we can easily calculate the average volume of a spinosal cell:

$$< v_s >= (v_b + v_g)/2 = v_b(1+g)/2 = 2.16 v_b \tag{2}$$

We assign this average volume to every spinosal cell, which allows us to calculate the thickness of the spinosal layer at any time from the number of spinosal cells at that time. As explained above, knowing the thickness of the spinosal layer at any time is sufficient to determine when a spinosal cell makes a transition to a granular cell.

Using an average volume of spinosal cells also simplifies the relationship between the mean TA-cell cycling time and the mean time t_0 required in our kinetic simulation to produce a fully developed via epidermis, which marks the beginning of a corneal layer by exposed to the

liquid-air interface. If the confluent basal-cell population is N and a fraction p of basal cells is cycling with a mean time T_c, then

$$t_0 = (T_c / p)(N_s / N + N_g / N) \tag{3}$$

where N_s and N_g are the number of spinosal and granular cells, respectively, in the fully developed spinosal and granular layers. Since $N = A\Delta_b/v_b$, where A is the area of epidermis being simulated, $N_s = A\Delta_s/\langle v_s \rangle$, and $N_g = A\Delta_g/v_g$, where Δ_g is the thickness of the granular layer, Eq. (3) becomes

$$t_0 = (T_c / p)[(\Delta_s / \Delta_b)(v_b / \langle v_s \rangle + (\Delta_g / \Delta_b)(v_b / v_g)] \tag{4}$$

Taking the average of 7 and 10 days as the typical time when the corneal layer begins [15], Eq. (4) predicts the mean TA cycling time of 31.2 h. This completes the parameter estimates for our kinetic simulation.

6. Effect of corneal screening on irradiation of the viable epidermis

The results of our kinetic simulation of epidermis development shown in **Figure 7** together with the estimate of 39 ± 1.41 μm for corneal layer thickness at 20 days postseeding of keratinocytes onto the dermal substrate enable the calculation of the protection that the corneal layer provides to live cells in the viable epidermis. We only model radiation exposure delivered after day 8.5, model radiation exposures delivered after day 8.5, the day selected in our model for first appearance of the corneal layer based on information from MatTek [15] that viable epidermis (basal, spinosal, and granular layers) is completed 7–10 days postseeding of keratinocytes onto the dermal substrate.

The thickness of the corneal layer on the day of irradiation was obtained from the results for cell count in the corneal layer, shown in **Figure 7**, after combining several simulations to reduce random fluctuations and normalizing to a thickness of 39 μm on day 20. From day 8.5 to about day 25, the increase in corneal thickness is linear. Beyond day 30, its thickness is constant since the replication capacity of the basal layer has been exhausted.

Based on results from simulations of a 90-keV electron beam stopping in a liquid-water medium [11], we developed an interpolation procedure for the amount of energy deposited in a layer of a given thickness at a given depth in the medium. As shown in Section 4, a liquid-water medium is a reasonable approximation to the epidermis of skin, including the corneal layer. Hence, our interpolation procedure allows the accurate prediction of radiation exposure to specified regions of the epidermis without the computationally intense, event-by-event simulation of 90-keV electrons penetrating an aqueous medium. The dermal substrate, which is composed of human fibroblast in a collagen matrix, is thick enough to stop a 90-keV electron

beam; hence, we estimate the energy deposited in the dermal substrate as the residual energy of electrons if they are not stopped in the epidermis.

The curve in **Figure 9** referred to the left-hand vertical axis shows our prediction for the energy deposited in the combined spinosal and basal layers depending on the day when the tissue was treated relative to the seeding of keratinocytes onto the dermal substrate. Spinosal and basal layers contain most of the cells with nuclei and that are undergoing growth and replication; consequently, they are the most sensitive to radiation exposure.

The results shown in **Figure 9** allow for the shrinkage of the viable epidermis observed to start on day 19 but with little significance until day 23, with the exception of day 21 where shrinkage is greater than on days 20 or 22 (see **Table 1**). The energy deposited in layers that contain nucleated cells decreases from a value about 50 keV per incident electron for irradiation on day 8.5, when the corneum is just beginning to form, to a value about 1 keV for irradiation on day 25. The lack of smoothness in these calculations after day 18 is due to observed shrinkage of the viable epidermis that begins on day 19.

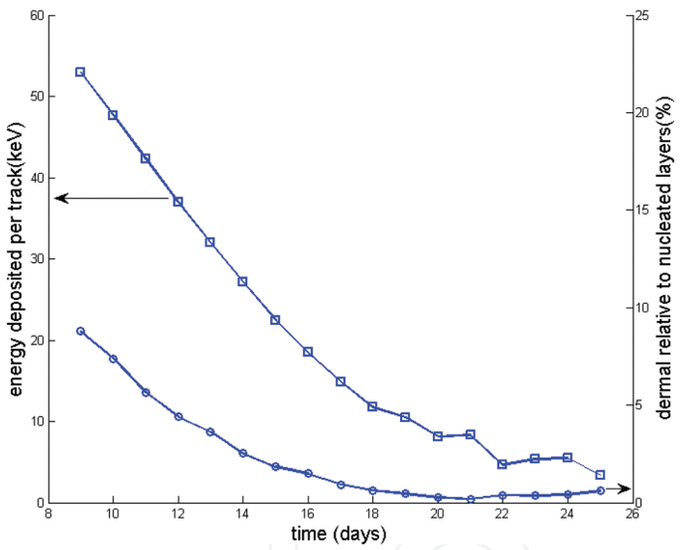

Figure 9. Effects of increasing corneum thickness on energy deposition in the combined basal and spinosum layers where keratinocytes are undergoing cell division and growth (left-hand vertical axis). The curve referred to the right-hand vertical axis is the energy deposited in the dermal substrate relative to that deposited in the combined basal and spinosal layers.

The curve in **Figure 9** referred to the right-hand vertical axis shows the energy deposited in the dermal substrate relative to that deposited in nucleated cells of the epidermis. When the corneal layer is thin, a significant fraction of the energy deposited reaches the fibroblast in the dermal substrate but this exposure is near zero for irradiation on day 21 when the corneal thickness has increased to about 40 μm. Comparing tissue responses at these different exposure times will not only show how screening by the corneal layer protects viable skin cells but may also reveal interactions between dermis and epidermis that are present when both components are exposed and absent when essentially all the radiation exposure is to epidermis alone.

Figure 9 suggests that irradiations performed around day 20 would deposit significant energy in the basal and spinosal layers with minimal exposure to the dermal substrate.

7. Conclusions

As artificial organotypic cell cultures become more widely used in research, their characterization becomes increasingly important. Morphology is a fundamental part of this characterization that can be accomplished through quantifiable microscopy techniques with sample preparation that preserves organ structure. The research described in this chapter concerned a part of artificial skin, the corneal layer, which is particularly prone to distortion in standard microtome-based slide preparation. To circumvent this difficulty, we correlated data from histologic staining methods [14] with data from 3D images of artificial-skin samples acquired by confocal microscopy [6]. However, this correlation of different types of microscope data required assumptions about the uptake of DNA stains by granular cells and a kinetic model to amplify the usefulness of confocal microscope data obtained at only one time point. In future work, direct measurements of corneal thickness can be obtained by new non-destructive techniques [20]. Despite these limitations on the available data, we achieved our objective of modeling the decrease in radiation exposure to live cells in the epidermis with increasing corneal thickness as the age of artificial skin samples increases.

Author details

Paola Pesantez-Cabrera[1], Cläre von Neubeck[2,3], Marianne B. Sowa[4] and John H. Miller[5*]

*Address all correspondence to: jhmiller@tricity.wsu.edu

1 School of Electrical Engineering and Computer Science, Washington State University, Pullman, WA, USA

2 German Cancer Consortium (DKTK), Dresden and German Cancer Research Center (DKFZ), Heidelberg, Germany

3 OncoRay, National Center for Radiation Research in Oncology, Faculty of Medicine and University Hospital Carl Gustav Carus, Technische Universität Dresden, Dresden, Germany

4 Space Biosciences Research Branch, NASA Ames Research Center, Moffett Field, CA, USA

5 School of Electrical Engineering and Computer Science, Washington State University Tri-Cities, Richland, WA, USA

References

[1] Griffith LG, Swartz MA. Capturing complex 3D tissue physiology in vitro. Nat Rev Mol Cell Biol 2006; 7:211–24.

[2] Belyakov OV, Mitchell SA, Parikh D, Randers-Pehrson G, Marino SA, Amundson SA, et al. Biological effects in unirradiated human tissue induced by radiation damage up to 1 mm away. Proc Natl Acad Sci U S A 2005; 102:14203–8.

[3] Sedelnikova OA, Nakamura A, Kovalchuk O, Koturbash I, Mitchell SA, Marion SA, et al. DNA double-strand breaks form in bystander cells after microbeam irradiation of three-dimensional human tissue models. Cancer Res 2007; 67:4295–302.

[4] Prise KM, Schettino G, Vojnovic B, Belyakov O, Shao C. Microbeam studies of the bystander response. J Radiat Res (Tokyo) 2009; 50 Suppl A:A1–6.

[5] Sowa MB, Chrisler WB, Zens KD, Ashjian EJ, Opresko LK. Three-dimensional culture conditions lead to decreased radiation induced cytotoxicity in human mammary epithelial cells. Mutat Res 2010; 687:78–83.

[6] von Neubeck C, Shankaran H, Geniza M, Kauer P, Robinson J, Chrisler W, et al., Integrated experimental and computational approach to understand the effects of heavy ion radiation on skin homeostasis. Integr Biol 2013; 5:1229–45.

[7] Gangatirkar P, Paquet-Fifield S, Li A, Rossi R, Kaur P. Establishment of 3D organotypic cultures using human neonatal epidermal cells. Nat Protoc 2007; 2:178–86.

[8] Vaughan MB, Ramirez RD, Brown SA, Yang JC, Wright WE, Shay JW. A reproducible laser-wounded skin equivalent model to study the effects of aging in vitro. Rejuvenation Res 2004; 7:99–110.

[9] Hei TK, Ballas LK, Brenner DJ, Geard CR. Advances in radiobiological studies using a microbeam. J Radiat Res (Tokyo) 2009; 50 Suppl A: A7–12.

[10] Zermeno A, Cole, A. Radiosensitive structures of metaphase and interphase hamster cells as studied by low-voltage electron beam irradiation. Radiat Res 1969; 39:669–84.

[11] Miller JH, Suleiman A, Chrisler WB, Sowa MB. Simulation of electron beam irradiation of skin tissue model. Radiat Res 2011; 175:113–8.

[12] Yang F, Waters KW, Miller JH, Gristenko MA, Zhao R, Du X, et al Phosphoproteomic profiling of human skin fibroblast cells reveals pathways and proteins affected by low doses of ionizing radiation. PLoS One 2010; 5(11) e14152 DOI: 10.1371/journal.pone.0014152

[13] Mat Tek Corporation. The EpiDermFT™ skin model.http://www.mattek.com/pages/products/epidermft/October 2, 2012

[14] von Neubeck C, Geniza M, Kauer P, Robinson J, Chrisler W, Sowa MB. The effect of low dose ionizing radiation on homeostasis and functional integrity in an organotypic human skin model. Mut Res 2015; 775:10–18.

[15] Luna LG (ed). Manual of histologic staining methods of the armed forces institute of pathology. 3rd edition. McGraw-Hill, New York; 1968.

[16] Wilson WE, Nikjoo H. A Monte-Carlo code for positive ion track simulation. Radiat Environ Biophys 1999; 38:97–104.

[17] Dingfelder M, Hantke D, Inokuti M, Paretzke HG. Electron inelastic-scattering cross sections in liquid water. Radiat Phys Chem 1998; 53:1–18.

[18] Wilson WE, Miller JH, Lynch DJ, Lewis RR, Batdorf M. Analysis of low-energy electron track structure in liquid water. Radiat Res 2004; 161:591–6.

[19] Weigand DA, Haygood C, Gaylor JR. Cell layers and density of Negro and Caucasian stratum coreum. J Invest Dermatol 1974; 62:563–8.

[20] Mateus R, Abdalghafor H, Oliverira G, Hadgraft J, Lane ME. A new paradigm in dermatopharmacokinetics – confocal Raman spectroscopy. Int J Pharm 2013; 444:106–8.